

DOI: 10.1002/adma.200600001

Enhancement of Radiative Recombination in Silicon via Phonon Localization and Selection-Rule Breaking**

By Sylvain G. Cloutier, Chih-Hsun Hsu, Pavel A. Kossyrev, and Jimmy Xu*

Sustained efforts have been made in pursuit of efficient light emission from silicon.^[1,2] This is not an easy endeavor because of silicon's indirect band structure, which causes radiative recombination to be possible but disfavored as it requires the assistance of phonons with the right momentum to make up for the momentum mismatch between available electrons and holes. However, this so-called phonon-selection rule can be relaxed or broken by crystal-symmetry breaking or phonon localization,^[3,4] which could be generated in low-dimensional silicon nanostructures,^[4-6] or by high defect-center or dislocation concentration in crystalline silicon.^[3,7,8] Phonon confinement in silicon nanocrystals has been experimentally studied and is now relatively well understood.^[6,9-12] Recent studies of periodic, uniaxially nanopatterned, crystalline silicon structures on silicon-on-insulator (SOI) have previously shown laserlike characteristics at 1278 nm and cryogenic temperatures; these characteristics were attributed to A-center-mediated phononless recombination.^[13] In the present work, high-resolution cross-sectional micro-Raman spectroscopy indicates strong phonon localization in such nanoengineered silicon structures. Photocurrent and photoluminescence spectroscopy have been independently used to demonstrate that such phonon-localization effects also lead to a breaking of the phonon-selection rule in bulk silicon, and to enhanced radiative recombination and light emission at room temperature. High-resolution transmission electron microscopy (HRTEM) allows direct observation of regions with high structural-defect densities, which are responsible for phonon localization and crystal-symmetry breaking, located in the surface layer of the nanoengineered silicon.

The periodic nanopatterned silicon structure shown in the left inset of Figure 1a was fabricated in 205 nm thick undoped electronic-grade crystalline SOI using a highly uniform self-assembled nanopore array as an etch mask. The anodic aluminum oxide (AAO) nanopore template was fabricated by a two-step anodization process under conditions described in

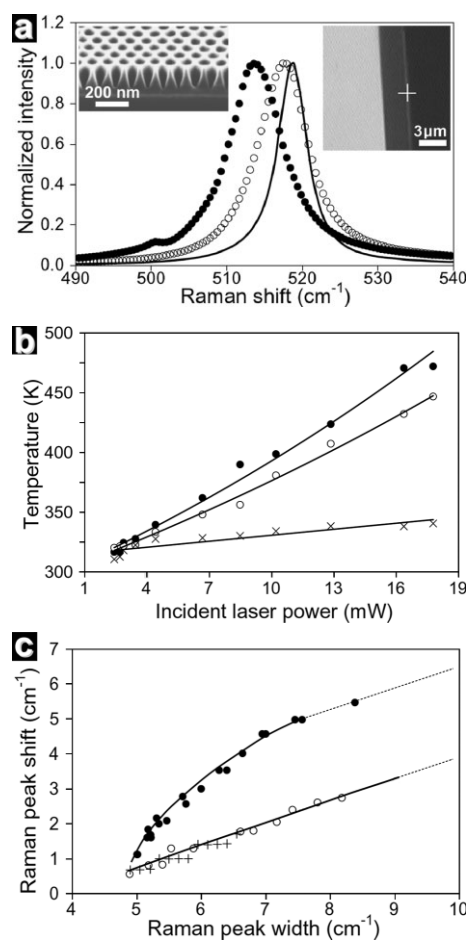


Figure 1. a) Raman spectra measured from bulk undoped silicon (line spectrum), the original unpatterned SOI (○), and the nanoengineered SOI structure (●). The left inset shows a 60° cross-sectional scanning electron microscopy (SEM) image of the periodically nanostructured crystalline silicon structure on SOI. The right inset shows a side view of a typical SOI sample in the Raman microscope at a 100× magnification. The cross indicates the optically excited top-layer region. b) Evolution of sample temperature as a function of the incident 532 nm laser power for bulk silicon (x), the original unpatterned SOI (○), and the nanoengineered SOI structure (●). c) Downshift of the Raman peak as a function of its associated spectral width (shift-width evolution) for the nanostructured (●) and original unpatterned SOI (+) samples. Also plotted are the results obtained for the same nanostructured SOI sample after a brief (8 min) thermal oxidation at 980 °C (○).

[*] Prof. J. Xu, S. G. Cloutier, C.-H. Hsu, Dr. P. A. Kossyrev
Division of Engineering and Department of Physics
Brown University
Providence, RI 02912 (USA)
E-mail: Jimmy_Xu@brown.edu

[**] We acknowledge support from DARPA and ONR. S. G. C. and J. X. are thankful to NSERC and the Guggenheim Foundation, respectively, for support in the form of fellowships and to Dr. Marian Tzolov for fruitful discussions and help with the photocurrent spectroscopy measurements.

the Experimental section.^[14-16] Grown to a thickness of 750 nm, such a nanopore mask was placed atop the SOI layer, which was insulated from the thick silicon substrate by a 3 μm

layer of silicon oxide. The nanoengineered silicon structure was obtained by using the AAO as a mask for pattern transfer using chlorine-based reactive-ion etching (RIE). The AAO mask was then removed by sonication.

Results from high-resolution cross-sectional phonon-spectroscopy measurements are shown in Figure 1a. The resulting approximately 1 μm diameter excitation spot size and the thick (3 μm) insulator layer allows the Raman spectrum from the top sub-micrometer silicon layer to be spatially distinguishable from that of the bulk silicon substrate by focusing the excitation laser beam on the topmost 205 nm thick SOI layer, as shown in the right inset of Figure 1a. The Raman spectrum of the original unpatterned SOI reference sample exhibits asymmetric broadening and a slight downshift in wave number compared with bulk silicon, which is expected because of the presence of intrinsic strain in the SOI.^[17] A much greater downshift of the Raman peak and further broadening are observed in the nanopatterned silicon structure on SOI. This cannot be explained by intrinsic built-in strains or Fano resonances only;^[8,10] however, it was previously shown that phonon-localization effects can cause such a significant downshift and broadening of the phonon line of silicon.^[5,6,18] A critical factor to consider is laser-induced heating, which could also lead to an additional downshift and broadening of the phonon line.^[10,12] A simple way to probe this contribution in situ is to simultaneously record the Stokes and anti-Stokes vibrational lines in the Raman spectra, since the intensity ratio of both phonon lines can be directly related to the sample temperature by Boltzmann statistics.^[18] Figure 1b displays the evolution of temperature with the power of the 532 nm excitation for the nanopatterned SOI structure, the original unprocessed SOI, and bulk silicon. As one may anticipate—given that the thermal conductivity of bulk Si is two orders of magnitude higher than that of SiO_2 (156 vs. 1.36 $\text{W m}^{-1} \text{K}$, respectively^[19,20])—the original unpatterned SOI heats up more than bulk silicon since its capacity to dissipate heat is effectively limited to two dimensions. The nanopatterned silicon structure on SOI shows a slightly increased laser-induced heating at high excitation powers due to a lower thermal mass and more spatially limited heat dissipation.

To dissociate the contribution of the laser-induced heating, the downshift of the phonon peak as a function of its associated width (i.e., shift-width evolution) has been plotted, as shown in Figure 1c. The region of nonlinear evolution observed for the nanopatterned silicon structure at low excitation power (or low sample temperature) indicates that the phonon line downshifts and broadens at different rates as the excitation power is increased, a clear signature of phonon-localization effects.^[6,18] At high excitation powers, this evolution becomes linear, marking out a laser-heating-dominated regime. It was found that the shift-width evolution became purely linear after a brief (8 min) dry-oxidation treatment at 980 $^\circ\text{C}$, which consumed a 4–6 nm layer at the interface, indicating that the phonon-localization effect vanished completely, and suggesting that such an effect occurs in the surface layer of the nanopatterned silicon.^[18]

Spatial phonon localization is expected to result in a broadening in momentum, leading to relaxation of the phonon-selection rule in bulk silicon and enhanced radiative recombination.^[4,6] Therefore, the intensity of the main free-exciton peak in the photoluminescence spectrum was measured as a function of the power density of the incident 514 nm pump, as shown in Figure 2a. This evolution, which should be linear for an ideal system, is limited by thermal effects and nonradiative recombination at high and low pump powers, respectively.^[21]

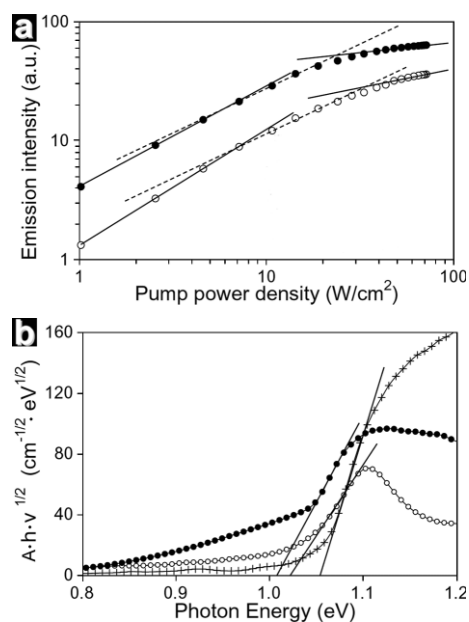


Figure 2. a) Evolution of free-exciton recombination photoluminescence intensity as a function of the incident pump power density for both the nanopatterned (●) and the original unprocessed SOI (○) samples. b) Photocurrent spectroscopy measurements for bulk silicon (+), original unpatterned SOI (○), and nanoengineered SOI (●).

This translates into deviation from the ideal linear behavior, as observed in Figure 2a for both the nanostructured and the original unpatterned SOI samples. The stronger deviation observed for the nanopatterned sample at high pump powers suggests more laser-induced heating, which is consistent with the results obtained from Raman spectroscopy. In addition, the near-ideal linear evolution at low pump powers indicates significantly suppressed nonradiative recombination in the nanopatterned SOI sample.^[21]

Additional insight into the phonon-localization effects can be gained by photocurrent spectroscopy measurements, which probe the states involved in upward optical transitions. Figure 2b compares the photocurrent spectra obtained for bulk undoped silicon, original unpatterned SOI, and the nanopatterned silicon structure on SOI. For indirect-bandgap semiconductors, the absorption coefficient, A , can be related to the incident photon energy, $h\nu$ (where h is Planck's constant, ν is the photon frequency), the bandgap energy, E_g , and the main longitudinal-optical phonon energy corresponding to the band-structure's k -mismatch, E_{LO} , via the relation

$Ahv = B(E_g + E_{LO} - hv)^2$, where B is an energy-independent physical parameter. This relation is used to produce the linear fit for the absorption band-edge data shown in Figure 2b, where B corresponds to the slope of the fit.^[22] Therefore, the intercept of the linear fit on the abscissa (horizontal axis) corresponds to an incoming photon energy equal to the sum of the bandgap energy and the main phonon energy ($E_{\text{photon}} = hv = E_g + E_{LO}$).^[23] On comparing the results for unpatterned SOI and bulk silicon, one notices that the intercept for the unpatterned SOI is slightly shifted towards lower photon energies. This can be attributed to the intrinsic material strain in SOI, which is also responsible for the asymmetric broadening towards lower wavenumbers observed in the phonon-spectroscopy measurements.^[17] A further decrease in the intercept value is observed for the nanopatterned SOI sample, along with a substantial increase in the phonon-absorption band tail,^[23] which is consistent with significant relaxation of the phonon-selection rule. Together, the photocurrent and photoluminescence spectroscopy measurements provide independent support to relaxation of the phonon-selection rule that was concluded from the Raman spectroscopy study, which, in turn, explains the radiative-recombination enhancement in the nanopatterned sample.

The fact that brief thermal oxidation removed the phonon-localization Raman signature strongly suggests that the source of the effect itself is localized in a thin (4–6 nm) surface layer around the cylindrical nanohole. To visualize the nanopatterned silicon surface layer, HRTEM was used for direct probing of the local atomic structure. The HRTEM image shown in Figure 3 clearly indicates the presence of regions

with high densities of structural defects located in the nanopatterned silicon surface layer. Defect-volume densities as high as 10 % were observed. It is known that high densities of structural defects could lead to phonon-localization effects.^[3,7,8] Our results provide direct confirmation that silicon structural defects are indeed present, enabling phonon-localization by breaking of the long-range crystal symmetry and, thereby, enhancing radiative recombination observed at room temperature in the periodically nanopatterned crystalline silicon structures. It is worth noting that some of these structural defects, such as A-centers, are emissive themselves.^[24] A-centers have been known to give rise to phononless radiative recombination at cryogenic temperatures, and are responsible for the stimulated emission and optical gain at 1278 nm reported in a previous study on similar nanoengineered silicon structures.^[13] However, as shown in this work, phonon localization and relaxation of the phonon-selection rule in bulk silicon also accounts for the enhanced radiative recombination observed at room temperature that has been enabled through nanoengineering.

In summary, we observed and studied phonon-localization effects in novel periodic uniaxially nanopatterned silicon structures on SOI fabricated using a highly ordered array of nanopores as a mask. It has been previously suggested that localization effects should lead to breaking of the phonon-selection rule in bulk silicon and to radiative-recombination enhancement. Indeed, photoluminescence spectroscopy shows that the balance between radiative and nonradiative recombination has been improved, and photocurrent spectroscopy demonstrates a significant relaxation of the phonon-selection rule. Dry-oxidation thermal treatment reveals that phonon localization occurs in the surface layer of the nanostructured silicon. HRTEM provides direct observation of regions with high densities of structural defects located in the surface layer of the nanopatterned structure. These structural defects, most likely silicon vacancies, are directly responsible for the unique light-emission properties reported previously at cryogenic temperatures in similar nanostructures,^[13] and for the phonon localization and enhanced radiative recombination at room temperature reported in this work. Similar phonon-confinement effects might also provide a partial explanation for enhanced light-emission properties previously observed using nanostructuring or implantation,^[25,26] leading to highly dislocated crystalline silicon structures. Given the importance of breaking the phonon-selection rule to achieve light-emission enhancement in silicon and other indirect-bandgap materials, we believe the findings presented here provide physical insight and offer useful guidelines to controllably modify the optical properties of indirect semiconductors through defect-engineering.

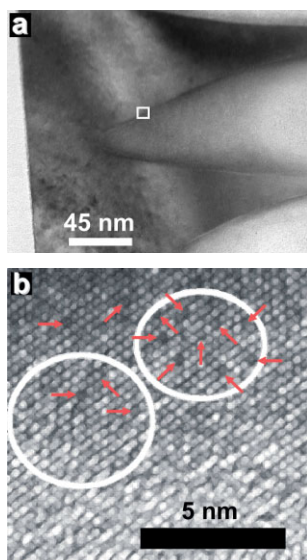


Figure 3. a) Low-magnification TEM image of the cross-section of the nanopatterned silicon layer. b) HRTEM image of the nanopatterned SOI surface-layer region identified by the rectangle in the center of the low-magnification image (a). The circles highlight regions with high concentrations of structural defects, a few of which are identified by the red arrows. The blurriness in the bottom region of the figure is attributed to the cylindrical geometry of the pore structure and the limited depth of focus.

Experimental

The nanopatterned silicon-on-insulator (SOI) structure was fabricated using a commercial SOI wafer from SOITEC Inc. The top-most 205 nm thick silicon $\langle 100 \rangle$ layer was separated from the thick silicon

substrate by a 3 μm thick silicon-oxide insulating layer. The anodic aluminum oxide (AAO) periodic nanopore array template was fabricated by first anodizing an annealed 5N (99.999 % purity) aluminum sheet in oxalic acid solution by applying a 40 V anodization voltage. The anodized aluminum layer was then dissolved in a H_3PO_4 -based solution and the anodization step was repeated under the same conditions for 9 min, leading to a 750 nm thick highly ordered AAO nanopore membrane being formed on the aluminum sheet. The AAO nanopore array was lifted off from the aluminum using a HgCl_2 solution for 30 min. The freestanding AAO mask was then deposited atop the SOI wafer. The AAO periodic nanopore pattern was transferred to the silicon using reactive-ion etching (RIE). The etching recipe includes 100 W rf power, 5 sccm BCl_3 , 20 sccm Cl_2 , 50 mTorr pressure (1 Torr \approx 133 Pa), and a 6 min etching time. After RIE, the AAO mask was removed in an ultrasonic bath.

SEM images of the nanopatterned SOI structure's cross section were taken at 1 kV using a LEO microscope model 1530VP. Micro-Raman spectroscopy measurements were performed using a Thermo-Nicolet Almega Raman microscope at an excitation wavelength of 532 nm, a maximum laser power of 20.4 mW, and a magnification of 100 \times . A built-in set of neutral-density filters allowed automated control of the excitation laser power. The photocurrent spectroscopy measurements were performed using a Bruker Equinox 55 Fourier transform IR (FTIR) spectrometer and the photoinduced current was collected using electron-beam-evaporated gold electrodes separated by a 200 μm gap, which were deposited on the surfaces of the samples. Finally, a LEO 1530 field-emission scanning electron microscope was employed to observe the morphology of the nanopatterned silicon structure. The microstructure of the nanopatterned silicon was studied using HRTEM. Cross-sectional HRTEM specimens were prepared by mechanical thinning. Bright-field high-resolution images, as well as electron diffraction patterns, were recorded using a JEOL JEM-2010 TEM operated as 200 kV.

Received: January 2, 2006
Final version: February 6, 2006

- [1] *Towards the First Silicon Laser* (Eds: L. Pavesi, S. Gaponenko, L. Dal Negro), Kluwer, Dordrecht, The Netherlands **2003**.
[2] M. Salib, L. Liao, R. Jones, M. Morse, A. Liu, D. Samara-Rubio, D. Alduino, M. Paniccia, *Intel Tech. Jour.* **2004**, *8*, 143.

- [3] P. T. Landsberg, *Solid-State Electron.* **1967**, *10*, 513.
[4] D. Kovalev, H. Heckler, G. Polisski, F. Koch, *Phys. Status Solidi B* **1999**, *215*, 871.
[5] H. Richter, Z. P. Wang, L. Ley, *Solid State Commun.* **1981**, *39*, 625.
[6] I. H. Campbell, P. M. Fauchet, *Solid State Commun.* **1986**, *58*, 739.
[7] M. Chandrasekhar, H. R. Chandrasekhar, M. Grimsditch, M. Cardona, *Phys. Rev. B* **1980**, *22*, 4825.
[8] N. H. Nickel, P. Lengsfeld, I. Sieber, *Phys. Rev. B* **2000**, *61*, 015 558.
[9] J. Zi, H. Buscher, C. Falter, W. Ludwig, K. Zhang, X. Xie, *Appl. Phys. Lett.* **1996**, *69*, 200.
[10] S. Piscanec, M. Cantoro, A. C. Ferrari, J. A. Zapien, Y. Lifshitz, S. T. Lee, S. Hofmann, J. Robertson, *Phys. Rev. B* **2003**, *68*, 241 312.
[11] M. S. Hybertsen, *Phys. Rev. Lett.* **1994**, *72*, 1514.
[12] N. Fukata, T. Oshima, K. Murakami, T. Kizuka, T. Tsurui, S. Ito, *Appl. Phys. Lett.* **2005**, *86*, 213 112.
[13] S. G. Cloutier, P. A. Kossyrev, J. Xu, *Nat. Mater.* **2005**, *4*, 887.
[14] J. Liang, H. Chik, A. Yin, J. Xu, *J. Appl. Phys.* **2002**, *91*, 2544.
[15] A. P. Li, F. Müller, A. Birner, K. Nielsch, U. Gösele, *J. Appl. Phys.* **1998**, *84*, 6023.
[16] H. Masuda, H. Yamada, M. Satoh, H. Asoh, M. Nakao, T. Tamamura, *Appl. Phys. Lett.* **1997**, *71*, 2770.
[17] J. Camassel, L. A. Falkovsky, N. Planes, *Phys. Rev. B* **2000**, *63*, 035 309.
[18] S. G. Cloutier, R. S. Guico, J. M. Xu, *Appl. Phys. Lett.* **2005**, *87*, 222 104.
[19] *CRC Materials Science and Engineering Handbook* (Eds: J. F. Shackelford, W. Alexander), CRC Press, London **2001**.
[20] *Properties of Crystalline Silicon* (Ed: R. Hull), IEEE, New York **2000**.
[21] I. Schnitzer, E. Yablonovitch, C. Caneau, T. J. Gmitter, A. Scherer, *Appl. Phys. Lett.* **1993**, *63*, 2174.
[22] T. P. Pearsall, H. Polatoglou, H. Presting, E. Kasper, *Phys. Rev. B* **1996**, *54*, 1545.
[23] C. Kittel, *Introduction to Solid State Physics*, Wiley, New York **1996**.
[24] R. J. Spry, W. D. Compton, *Phys. Rev.* **1968**, *175*, 1010.
[25] W. L. Ng, M. A. Lourenço, R. M. Gwilliam, S. Ledain, G. Shao, K. P. Homewood, *Nature* **2001**, *410*, 192.
[26] M. J. Chen, J. L. Yen, J. Y. Li, J. F. Chang, S. C. Tsai, C. S. Tsai, *Appl. Phys. Lett.* **2004**, *84*, 2163.